Supplementary Information for

Programmable assemblies of photothermal anisotropic micromotors for multimodal motion

Wenchang Zhao, Shiyu Wang, Ying Zhou, Yanhong Li, Shuxian Tang, Yutong Zheng, Pingan Zhu*

*Corresponding author. e-mail: pingazhu@cityu.edu.hk

This file includes:

Note S1

The capillary length λ_c serves as a lengthscale related to gravity and surface tension. It is a fundamental physical quantity that governs the behavior of the meniscus, emerging when body forces (gravity) and surface forces (Laplace pressure) are in equilibrium. For a spherical droplet with a radius of λ_c, Laplace pressure P_L is generated due to surface tension γ:

$$P_L = 2\frac{\lambda_c}{\gamma}$$

The pressure P_g is generated due to gravity:

$$P_g = \rho g h = 2\rho g\, \lambda_c$$

where ρ is the density of the droplet, g is the gravitational acceleration, and h is the height of the droplet.

When Laplace pressure and gravity pressure are in equilibrium ($P_L = P_g$).

$$\lambda_c = \sqrt{\frac{\gamma}{\rho g}}$$

At 20 °C, the surface tension of water is 72.8 mN/m, resulting in a capillary length for water of around 2.7 mm.

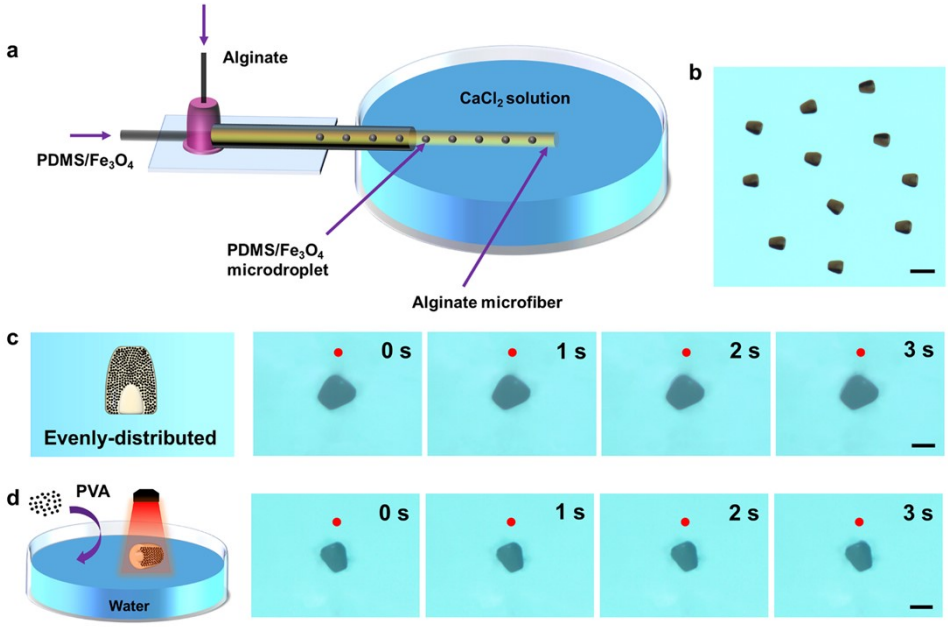

Fig. S1 Fabrication and Motion of Micromotors. (a) Schematic of the experimental setup for fabricating micromotors using microfluidic technology. (b) Image displaying dozens of micromotors, highlighting their high uniformity in both shape and size. (c) Illustration of the stationary behavior of a micromotor with uniformly distributed Fe_3O_4 nanoparticles (Fe_3O_4-NPs). (d) Observation of the stationary state of a micromotor in the presence of 0.2 wt% polyvinyl alcohol (PVA) added to the water. The scale bars are 1 mm in (b), 500 μm in (c) and (d). Artificially added red dots in (c) and (d) aid in visualizing the micromotor's motion.

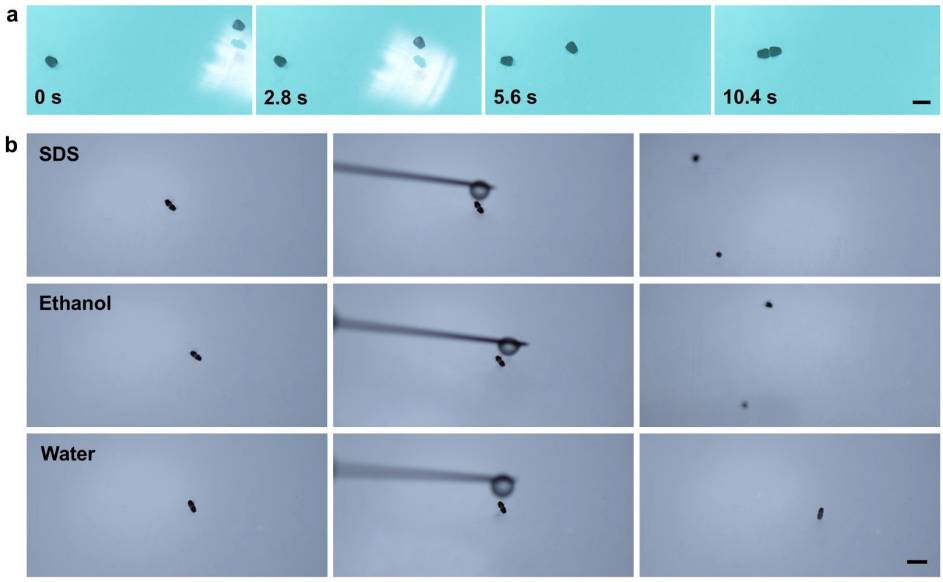

Fig. S2 Self-Assembly and Disassembly of Micromotors. (a) Self-assembly of micromotors facilitated by reducing the spacing between micromotors under NIR illumination. (b) Disassembly of micromotors by depositing droplets of low-surface-tension liquids. Low-surface-tension liquids such as 2% SDS solution and ethanol effectively disassemble the assemblies, whereas high-surface-tension water does not. The scale bars are 1 mm in (a) and 2 mm in (b).

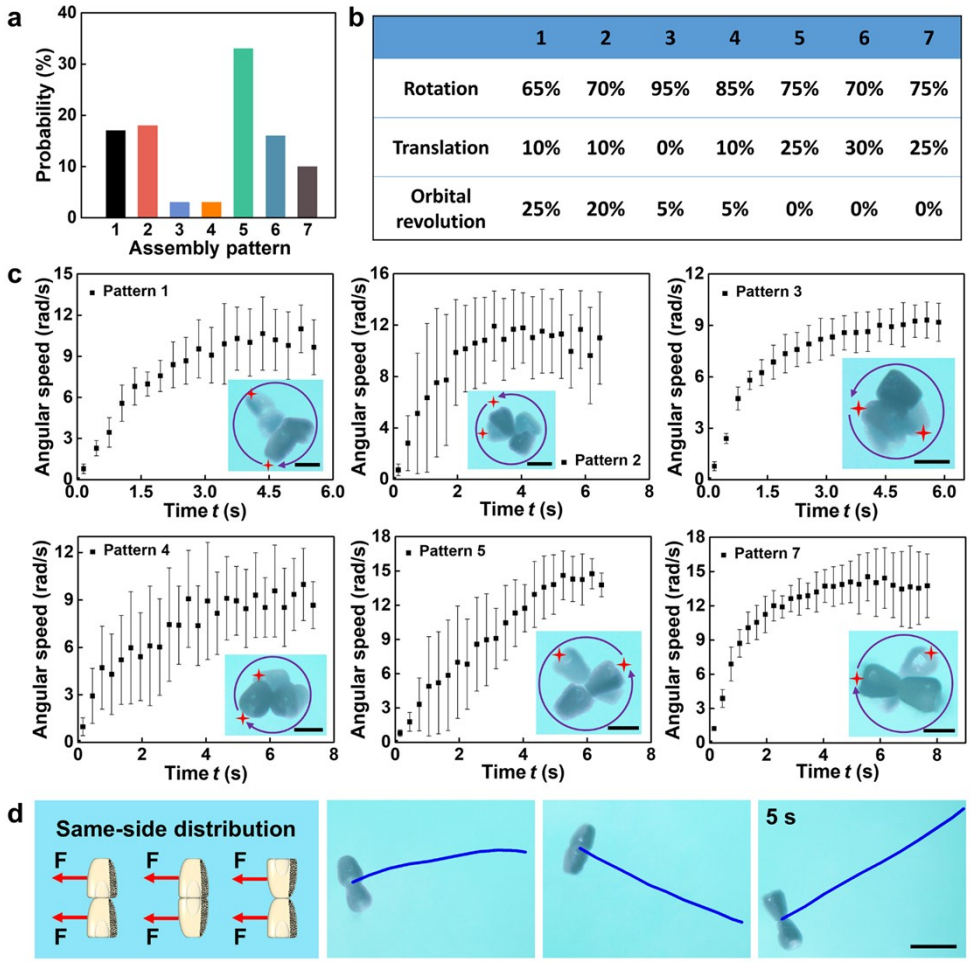

	1	2	3	4	5	6	7
Rotation	65%	70%	95%	85%	75%	70%	75%
Translation	10%	10%	0%	10%	25%	30%	25%
Orbital revolution	25%	20%	5%	5%	0%	0%	0%

Fig. S3 Movement of double-motor self-assembly. (a) The occurrence probabilities of the seven patterns. (b) Under NIR irradiation, the types of motion exhibited by the seven patterns and their corresponding probabilities, with twenty tests for each pattern. (c) The relationship between angular speed and time *t* for six patterns. The inset illustrates the corresponding superimposed snapshots of rotational motion. The time interval between each superimposed image is 1 s. (d) Illustration of the translational motion for micromotor assemblies with Fe_3O_4-NPs distributed on the same side. The scale bars are 500 μm in (c) and 1 mm in (d).

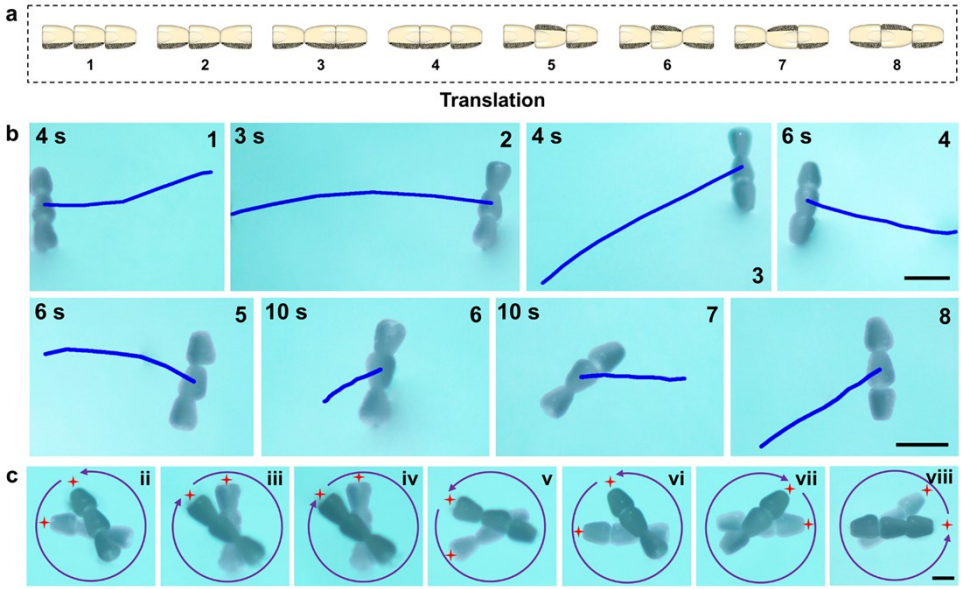

Fig. S4 Movement of triple-motor self-assembly. (a) Eight patterns of triple-motor self-assembly exhibiting translational motion. (b) Motion trajectories of the eight patterns in (a). Scale bar, 1 mm. (c) Superimposed images showing the rotation of patterns ii-viii. The scale bar is 500 μm. The time interval between each superimposed image is 0.8 s.

Fig. S5 Assembly of Micromotors into Sophisticated Patterns. English letters, Chinese characters, and numbers with encoded information are assembled with the assistance of a magnetic field. Scale bar, 2 mm.

Table S1. Representative examples of photothermal-driven micro/nanomotors.

Material type	Method	Preparation steps	Photothermal strategy	Illumination type	Motion modes	maximum speed	Self-assembly	Ref
Carbonized PDMS	Direct laser writing	One	Marangoni effect	Localized focusing/Full-area	Translation /Rotation	1.57 rad/s	No	49
Carbonaceous nanobottle	soft-template-based polymerization	Two	thermophoresis effect	Full-area	Translation	25 μm/s	No	50
TiO_2/Pt Janus micromotors	Magnetron sputtering	Two	natural and Marangoni convection	Full-area	Translation	70 μm/s	Yes, but lack of control and order	34
Gold and platinum nanoparticles modified microtubules	Template-assisted layer-by-layer assembly	Three	bubble recoil	Full-area	Translation	63 μm/s	No	51
Substrates integrated with MXene	Chemical exfoliation and coating	Two	Marangoni effect	Localized focusing	Translation Rotation	Not provided	No	52
This work	Microfluidics	One	Marangoni effect	Full-area	Translation Revolution Rotation	1.62 mm/s 1.95 mm/s 17.4 rad/s	Yes, customizable	

Movie S1. Translation and revolution motions of a single micromotor under NIR irradiation. The micromotor exhibits two distinct motion modes: translation and revolution when exposed to NIR light.

Movie S2. Flow field around the micromotor visualized with fluorescent particles. As the micromotor moves under NIR light, the surrounding fluorescent particles spontaneously move away from it, with the more intense movement observed on the Fe_3O_4-NPs side due to the higher temperature.

Movie S3. On-demand motion by controlling the on and off of light. Under NIR irradiation, the micromotor shows notable displacement, which is halted when the NIR is turned off. Upon reactivation of the NIR, immediate motion occurs, demonstrating a rapid response.

Movie S4. Self-assembly process of micromotors driven by capillary interactions. This process involves three scenarios: (1) when the axes of two micromotors are aligned, they directly combine into a chain; (2) when one end of a micromotor is tilted and submerged underwater, a non-chain structure is formed; and (3) when two micromotors are placed in parallel, they spontaneously rotate to align and form a chain.

Movie S5. Using NIR to drive micromotors closer for self-assembly. When the micromotors are too far apart, NIR is used to bring them closer, after which self-assembly occurs spontaneously due to capillary interactions.

Movie S6. Disassembly of the assembled structures by adding droplets. The addition of a 2% SDS solution or ethanol causes disassembly of the micromotor assembly, while water has no effect, confirming that the disassembly is not due to

impact.

Movie S7. Rotational motion of seven double-motor self-assembly patterns. Seven different patterns of double-motor self-assemblies exhibit rotational motion when exposed to NIR light.

Movie S8. Rotational motion of triple-micromotor assemblies. Eight distinct triple-micromotor assemblies demonstrate rotational motion, with Fe_3O_4-NPs distributed at opposite sides of the two ends.

Movie S9. Combined motion modes of quadruple- and quintuple-micromotor assemblies. Assemblies with micromotors featuring different Fe_3O_4-NP distributions exhibit unique combined motion modes, incorporating both translational and rotational movements.

Movie S10. Programming micromotor self-assembly using external fields. Microparticles self-assemble into short chains of specific lengths, which are then positioned and combined using light and magnetic fields to create complex patterns, such as English letters and Chinese characters.

Movie S11. Combined light and magnetic fields for sophisticated micromotor motion. The light field induces translational motion, while the magnetic field provides directional guidance to steer the micromotor.